BioSig: A Bioinformatic System for Studying the Mechanism of Inter-Cell Signaling

B. Parvin, G. Cong, G. Fontenay, and J. Taylor
Computing Sciences
R. Henshall and M.H. Barcellos-Hoff
Life Scienses
Lawrence Berkeley National Laboratory
Berkeley, CA 94720

Abstract

Mapping inter-cell signaling pathways requires an integrated view of experimental and informatic protocols. BioSig provides the foundation of cataloging inter-cell responses as a function of particular conditioning, treatment, staining, etc. for either *invivo* or *invitro* experiments. This paper outlines the system architecture, a functional data model for representing experimental protocols, algorithms for image analysis, and the required statistical analysis. The architecture provides remote shared operation of an inverted optical microscope, and couples instrument operation with images acquisition and annotation. The information is stored in an object-oriented database. The algorithms extract structural information such as morphology and organization, and map it to functional information such as inter-cellular responses. An example of usage of this system is included.

1 Introduction

The challenge of the post-genomic era is functional genomics, i.e., understanding how the genome is expressed to produce myriad cell phenotypes. A phenotype is the result of selective expression of the genome in response to the microenvironment. To use genomic information to understand the biology of complex organisms, the biological responses and signaling pathways in cells need to be studied in context, i.e., within a proper tissue structure. In turn this information will then more accurately predict health effects such as those following exposure to ionizing radiation. This paper focuses on an imaging bioinformatic system used to map fundamental pathways for cell signaling in tissue. The signaling mechanism has a profound impact on cell division (mitosis), death (apoptosis), and organization. It is well-known that protein-protein interactions play an important role in biological processes. These interactions are the fundamental prerequisites for control of cell cycle, DNA replication, transcription, metabolism, and signal transduction. The ultimate decision of a cell to proliferate, differentiate or die is the response to integrated signals from the extracellular matrix (ECM), cell surface, growth factors and hormones. Our current aim is to understand how ionizing radiation alters tissue homeostasis. This is achieved by studying the effect of low-dose radiation on cellular microenvironment, inter-cell communication, and the underlying mechanisms. The dynamics of events initiated at the cellular level but acting on the tissue provides the key to manipulating the consequences of radiation exposure. Recent studies have shown that some of the signaling pathways occur via the cell adhesion system. Cell adhesion is the mechanism that a cell attaches itself to the ECM. By manipulating the ECM receptors on the cell, one can study changes in their response, morphologies, and organization as a function of time. One significant aspect of such studies is that changes in shape, response, and organization are statistical and a particular observation cannot take place on the same sample over time. It is therefore necessary to conduct large population studies and correlate distant features (measured from images) with annotation data.

We have developed a bio-informatics framework of integrated image acquisition, annotation, and hierarchical image abstraction to create a database that registers localization and intensity information about multiple targets along with positional references and morphological features. Statistical and visualization tools will be integrated to allow hypothesis testing and data mining. The organization of this paper is as follows. Section 2 provides a brief overview of the system architecture and database interaction. Section 3 outlines various components of the informatic system. Section 4 provides the detail of the image analysis algorithms. Section 5 outlines the details of a specific experiment. Section 6 concludes the paper.

*This work is supported by the Director, Office of Energy Science Research, with Office of Biological and Environmental Research, and Office of Computation and Technology Research, Mathematical, Information, and Computational Sciences Division, of the U. S. Department of Energy under Contract No. DE-AC03-76SF00098 with the University of California. The publication number is LBNL-46757. E-mail: parvin@media.lbl.gov. Web site is at http://vision.lbl.gov

2 Architecture

We have developed a system, named DeepView, to operate an inverted optical microscope in a collaborative fashion [8]. DeepView is a "Microscopy Channel" over the wide area network. A microscopy channel advertises a listing of available online microscopes, where users can seamlessly participate in an experiment, acquire expert opinions, collect and process data, and store this information in their electronic notebook. The channel is a collaborative problem solving environment (CPSE) that allows for both synchronous and asynchronous collaboration. The current testbed includes several unique electron and optical microscopes with applications ranging from material science to cell biology. We have studied current commercial CORBA services and concluded that three basic services are needed to meet the extensibility and functionality constraints. These include: Instrument Services (IS), Exchange Services (ES), and Computational Services (CS). These services sit on top of CORBA and its enabling services (naming, trading, security, and notification). IS provide a layer of abstraction for controlling any type of microscope. ES provide a common set of utilities for information management and transaction. CS provide the analytical capabilities needed for online microscopy and PSE. The overall architecture of this system is shown in Figure 1. DeepView provides a flat file mechanism for logging and storing annotation and image data, which is not adequate for efficient access of large scale data in a systematic way. A new addition to DeepView is the informatic framework for problem solving that includes an object oriented database for storage and retrieval. A key design decision has been not to provide a direct CORBA interface to the database at this point. This is due to the fact the current CORBA interfaces to OO databases are weak and not well supported by various vendors. The interface to the database is shown in Figure 2. It uses a browser to access the web-server and the database. The database supports some computational functionalities on metadata, however, all image analysis operations are performed with the computation services.

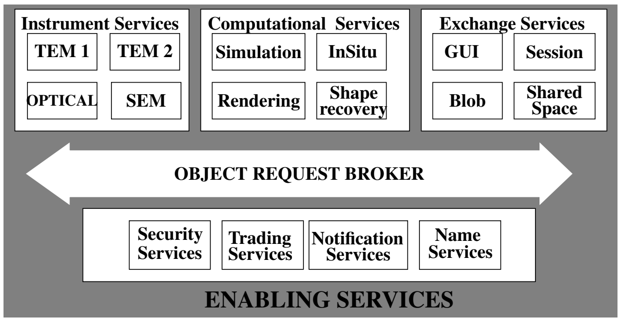

Figure 1: Interaction between OMG-defined Enabling Services and DeepView Services.

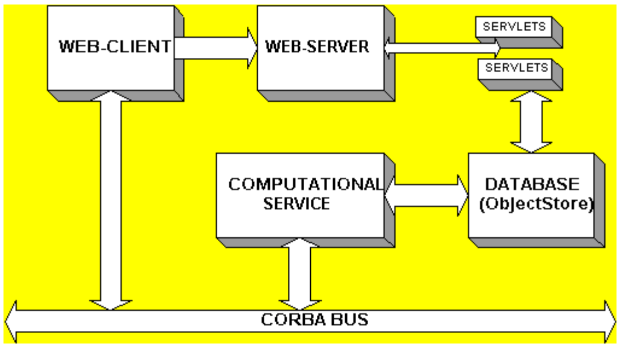

Figure 2: Interaction between user, data base, and computational services.

3 Informatics

The informatic system consists of three components. These include (1) data model, (2) presentation manager, and (3) query manager. These subsystems are decoupled for ease of development, testing, and maintenance. The purpose of the data model component is to capture required annotation data and couple them to computed representation of images for hypothesizing signaling pathways. The model is object oriented and allows bidirectional tracking of annotation and measured feature data. The presentation manager provides two distinct features. These include a mapping between data model and the user interface. The intent is to avoid hardwiring the user interface in favor of a more flexible interface that can be constructed at run time regardless of changes in the underlying data model. The second feature provides the display functionality of a particular query in either text or graphics. The query manager maps high level user queries to the Java objects that implement the data model. The intent is to simplify and hide detailed manipulation of the database from the end users. Each of these components are discussed in further details.

3.1 Data model

The data model, shown in Figure 3, is object-oriented and links a particular project to computed features from a collection of images. This link is bidirectional to allow tracking of information from any end point. Each project has its own database, which is linked to studies. A study consist of *invivo* or *invitro* experiments. *Invivo* experiments consists of animals (mostly mice in our experiments) that are conditioned and treated in a specific way. For example, treatment may include any number of antibodies, implants, radiation, or pharmaceuticals at a specific dosage and time. Tissue sections are then prepared from an organ at a specific thickness, then stained with primary and secondary antibodies. An antibody is a tool to study proteins. These stained samples are then imaged and pertinent features are computed. Likewise, *invitro* experiments use a similar protocol to prepare the samples for imaging and quantitative analysis.

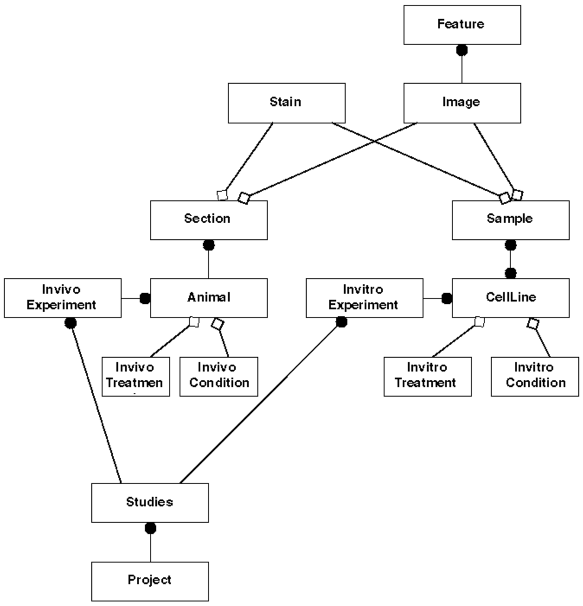

Figure 3: Data model for annotation of image data.

3.2 Presentation manager

The presentation manager has two features that includes browsing and updating, and displaying the result of a query function. The data model of Figure 3 is represented in XML and the presentation manager constructs a view into the database using this representation for browsing and updating. In this context, hardwiring of a GUI is bypassed in favor of a more flexible user interface. In general, such a mapping may create a complex implementation issue. However, we have simplified the presentation system to allow browsing and updating one layer at a time. A layer refers to navigation between an object and other objects that are linked through association, aggregation, and inheritance. The presentation manager maintains its own state and provides the required interaction between user and the database. Finally, the presentation manager displays the result of a query function in either text or graphics. The graphics include dose-response plots and scatter diagrams of computed features as a function of independent variables.

3.3 Query manager

The query manager provides a set of predefined operators to assist in hypothesis generation and testing. These operators aid to draw contrast between computed representation with different annotation data and perform a variety of statistical measures such as analysis of variance and principal component analysis. These operators allow signaling pathways to be deciphered for an eventual model reconstruction. An example of such a high level operator includes correlation of a particular computed feature (features) with respect to independent variable (variables). Such a high level operator *correlates* "area" feature between samples that have been treated with 2 Gy-levels of radiation and those that have not been radiated at all. This query is table driven and no scripting language is used for its entry. The query manager decodes such a complex user query to a set of database operations, computes the results, and returns the results to the presentation manager for display. The actual computation may include analysis of variance (for relating a particular measurement against number of independent samples) or PCA (for reducing the dimensionality of computed feature vector) for the display purposes.

4 Extraction of nuclei

Automatic delineation of cell nuclei is an important step in mapping functional activities into structural components in cell biology. The nuclei of interest reside in a thin layer that surround a particular type of capillary in the tissue. The intent is to build the necessary computational tools for large scale population studies and hypothesis testing. These nuclei may be clumped together, thus, making quick delineation infeasible. An example is shown in Figure 4(a)(b). Previous efforts in this area have been focused on thresholding, local geometries, and morphological operators for known cell size [11, 12]. Others have focused on an *Optimal Cut Path* that minimizes a cost function in the absence of shape, size, or other information [4, 15].

We propose an approach that utilizes both step-edge and roof-edge boundaries to partition a clump of nuclei in a way that is globally consistent. In this context, images are binarized and boundaries–corresponding to step edges–are recovered. Next, concave corners are extracted from polygonal approximation of the initial boundary segments. These corners provide possible cues to where two adjacent cells may come together. Furthermore, crease segments [6, 7, 13] provide additional boundary conditions for the grouping process. These crease segments correspond to trough boundaries between adjacent nuclei. A unique feature of our system is in hyperquadric representation of each hypothesis and the use of this representation for global consistency. The main advantage of such a parameterized representation–as opposed to polygonal representation–is better stability in shape description from partial information. In this fashion, each step-edge boundary segment belongs to one and only one cell while each roof-edge boundary segment is shared by two and only two cells. These initial hypotheses and their localized inter-relationship provides the basis for search in the grouping step. This is expressed in terms of an adequate cost function and minimized through dynamic programming. The final result of this computational step is then shown to a user for verification and elimination of false alarms.

In the remainder of this section, we will briefly re-

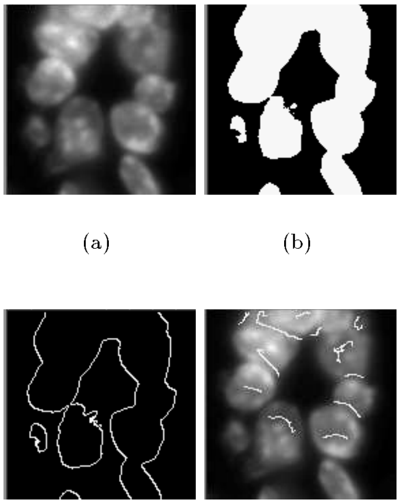

(a) (b) (c) (d)

Figure 4: An example of cell lines with the result of global and local operations: (a) original image; (b) threshold image; (c) boundary objects; and (d) local troughs.

view each step of the representation process and parameterization of each hypothesis in terms of hyperquadric. This will be followed by the details of the grouping protocol, results on real data, and concluding remarks.

4.1 Representation

The initial step of the computational process is to collect sufficient cues from local feature activities so that a set of hypotheses–not all of them correct–can be constructed for consistent grouping. These initial steps include thresholding, detection of concave points from boundary segments, extraction of crease segments from images, and hyperquadric representation of each possible hypothesis.

Binary thresholding extracts the clump patterns from the original image. The corresponding threshold can be obtained through simple histogram analysis or analysis of contrast histogram. This is a valid approach for fluorescence images because of absence of any shading artifact. The next step is to partition the clump silhouettes into segments that correspond to partial cell boundaries. Often the boundary between two adjacent nuclei is signaled by a concave point, that can be detected with corner detector. These corners are localized from the turning angle between adjacent line segments that are computed by polygonal approximation of the original contours.

4.1.1 Detection of crease boundaries

In grey images, crease points can be defined as local extremes of the principal curvature along the principal direction [6, 7, 14, 13]. It is well known that due to noise, scale, finite differential operators, and thresholds, it is very difficult to detect complete creases as shown in Figure 4(d). Images are enhanced through a variation of nonlinear diffusion to improve localization of crease points. The principal curvature and direction are then computed, using the standard forms, and crease points are linked to form curve segments.

4.1.2 Hyperquadric model

A brief introduction to hyperquadric fitting is included. A more detailed description can be found in [2, 3, 5]. A 2D hyperquadric is a closed curve defined by:

$$\sum_{i=1}^{N} |A_i x + B_i y + C_i|^{\gamma_i} = 1 \quad (1)$$

Since $\gamma_i > 0$, (1) implies that

$$|A_i x + B_i y + C_i| \leq 1 \quad \forall i = 1, 2, ..., N \quad (2)$$

which corresponds to a pair of parallel line segments for each i. These line segments define a convex polytope (for large γ) within which the hyperquadric is constrained to lie. This representation is valid across a broad range of shapes which need not be symmetric. The parameters A_i and B_i determine the slopes of the bounding lines and, along with C_i, the distance between them. γ_i determines the "squareness" of the shape.

The fitting problem is as follows. Assume that m data points $p_j = (x_j, y_j), j = 1, 2, ..., m$ from n segments ($m = \sum_{i=1}^{n} m_i$) are given. The cost function is defined as:

$$\epsilon^2 = \sum_{j=1}^{m} \frac{1}{||\nabla F_j(p_j)||^2}(1 - F_j(p_j))^2 + \lambda \sum_{i=1}^{N} Q_i \quad (3)$$

where $F_j(p_j) = \sum_{i=1}^{N} |A_i x_j + B_i y_j + C_i|^{\gamma_i}$, ∇ is the gradient operator, λ is the regularization parameter and Q_i is the constraint term [5]. The parameters A_i, B_i, C_i, γ_i are calculated by minimizing ϵ using the Levenberg-Marquard nonlinear optimization method [9] from a suitable initial guess [5]. Several examples of hyperquadric fitting to an initial set of partial segments are shown in Figure 5.

4.2 Grouping for nuclei

Let each clump be represented by n_b boundary segments $b_i, i = 1, ..., n_b$ and n_c crease segments $c_i, i = 1, ..., n_c$. We need to find a smaller segment set Φ_i for each nuclei. Next, we define a set $\tilde{\Phi}_i$ such that $\Phi_i \subseteq \tilde{\Phi}_i$. It is assumed that detecting $\tilde{\Phi}_i$ is trivial and $\tilde{\Phi}_i$ contains all the segments that have certain

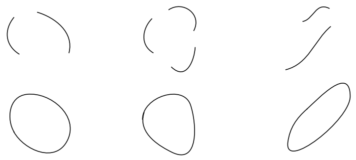

(a)

Figure 5: Fitting results for hyperquadrics.

possibilities to be part of the ith nucleus. Computing Φ_i from $\tilde{\Phi}_i$ is in fact subject to local, adjacency, and global constraint. It is under-constrained and the solution is not unique. Each possible solution is measured by the "goodness criteria" proposed in section 3.3 and the one with minimum cost determines the segmentation.

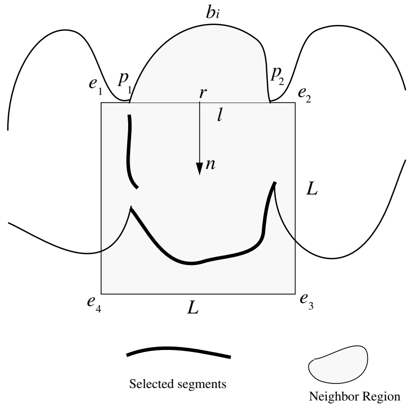

(a)

Figure 6: Neighborhood function

4.2.1 Neighborhood function

A neighborhood function is defined over a region for each b_i, as shown in Figure 6. Suppose that p_1 and p_2 are the end points of b_i and r is the line segment connecting them with $l = ||r||$ as the length. The neighborhood function is then defined as the combination of a fixed size bounding box (of size L) that extends and encloses concave points along the boundary. This procedure is simple, yet scale sensitive. However, it can be eliminated through constrained triangulation at a cost of additional computational overhead.

Thus, any segment $b_j, j = 1, ..., n_b$ or $c_j, j = 1, ..., n_c$ that resides in the bounding box is included in $\tilde{\Phi}_i$.

4.2.2 Search strategy

The key data structure in our approach is the *Assignment Matrix* $\mathcal{M}$. Each row of $\mathcal{M}$ indicates a possible cell. For the clump under investigation, we can construct up to n_b cells. Thus, $\mathcal{M}$ has n_b rows. Each column of $\mathcal{M}$ indicates a boundary or crease segment. Since each crease is shared by two cells, we assign two columns for it. Thus, $\mathcal{M}$ has $n_b + 2n_c$ columns. Let

$$\begin{aligned} s_j &= b_j, \quad 1 \leq j \leq n_b \\ s_{n_b+2j-1} &= s_{n_b+2j} = c_j, \quad 1 \leq j \leq n_c \end{aligned} \tag{4}$$

$\mathcal{M}$ is determined by

$$m_{ij} = \begin{cases} 1 & \text{if } s_j \in \tilde{\Phi}_i \\ 0 & \text{otherwise} \end{cases} \tag{5}$$

An example for construction of $\mathcal{M}$ for feature segments of Figure 7 is shown in Figure 8. For example, assume that

$$\begin{aligned} \tilde{\Phi}_1 &= \{b_1, c_1, b_4, b_5\} \\ \tilde{\Phi}_2 &= \{b_2, c_1, b_5, b_6\} \\ \tilde{\Phi}_3 &= \{b_3, b_6\} \\ \tilde{\Phi}_4 &= \{b_4, c_1, b_1\} \\ \tilde{\Phi}_5 &= \{b_5, c_1, b_2\} \\ \tilde{\Phi}_6 &= \{b_6, b_3\} \end{aligned} \tag{6}$$

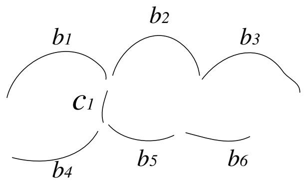

(a)

Figure 7: An example of boundary and crease segments

The ith row of $\mathcal{M}$ represents all possible segments that may be part of a nucleus. The jth column of $\mathcal{M}$ indicates all possible nuclei that s_j may belong to. The main constraint is to enforce sharing a crease segment between two different nuclei or not using this segment

	b_1	b_2	b_3	b_4	b_5	b_6	c_1	c_1
cell 1	1	0	0	1	1	0	1	1
cell 2	0	1	0	0	1	1	1	1
cell 3	0	0	1	0	0	1	0	0
cell 4	1	0	0	1	0	0	1	1
cell 5	0	1	0	0	1	0	1	1
cell 6	0	0	1	0	0	1	0	0

- - - - Path I
―――― Path II

(a)

Figure 8: Assignment matrix for features of Figure 7

at all for any nuclei. For example, path I in figure 8 indicates that

$$\begin{aligned} \Phi_1 &= \{b_1\} \\ \Phi_2 &= \{b_2, c_1, b_5\} \\ \Phi_3 &= \{b_3, b_6\} \\ \Phi_4 &= \{b_4\} \\ \Phi_5 &= \{c_1\} \\ \Phi_6 &= \phi \end{aligned} \tag{7}$$

$\Phi_i, i = 1, 2...$ are then fitted by hyperquadrics each of which is evaluated by the criteria proposed in the next section. Thus, the cell segmentation problem is equivalent to finding a best path with minimum cost. For example, the best path for Figure 7 is $Path\ II$ as shown in Figure 8, i.e.,

$$\begin{aligned} \Phi_1 &= \{b_1, c_1, b_4\} \\ \Phi_2 &= \{b_2, c_1, b_5\} \\ \Phi_3 &= \{b_3, b_6\} \\ \Phi_4 &= \phi \\ \Phi_5 &= \phi \\ \Phi_6 &= \phi \end{aligned} \tag{8}$$

The actual search process is based on dynamic programming [10, 1], where the local cost function is defined in the next section. The dynamic programming algorithm is essentially a multi-stage optimization technique where at each stage, or each iteration, the size of the path is increased by one set of feature segments. This process is repeated for each starting point in the assignment matrix, and the path with least cost is selected as final hypothesis.

4.2.3 Evaluation criteria

Although nuclei may have completely different morphology, we have some general information about their shapes and properties. This information enables us to compare different hyperquadrics, get rid of the undesirable ones, and reduce false alarms. The "goodness" criterion includes four terms: area A, shape S, overlap O and error C. Each is evaluated by its representative function E_A, E_S, E_O and E_C. The local cost is then given by $E_T = E_A + E_S + E_O + E_C$ with the intent of minimizing E_T over the entire set of hypotheses. The transition cost between two adjacent hypotheses is simply an exclusive consistency measure. E_A, E_S, E_O and E_C are computed as follows:

1. E_A. A is the area of the hyperquadric. A nucleus should neither be bigger than (A_b) nor smaller than (A_s).

$$E_A = \begin{cases} 0, & \text{if } A_s \le A \le A_b \\ 1 - e^{-\frac{A - A_b}{\sigma_A}} & \text{if } A > A_b \\ 1 - e^{-\frac{A_s - A}{\sigma_A}} & \text{if } A < A_s \end{cases} \tag{9}$$

   where we choose $A_b = L^2, A_s = \frac{1}{4}L^2$.

2. E_S. S defined as an aspect ratio as measured by the ratio of minor to major axes as shown in Figure 9(a). E_S is defined to favor perfect circles:

$$E_S = 1 - e^{-\frac{1-S}{\sigma_S}} \tag{10}$$

3. E_O. A hyperquadric may not always be enclosed by the cell clump. An overlap measure is defined as the ratio of area inside the clump to the total area of the hyperquadric. E_O is defined to favor larger values of O as shown in Figure 9(b):

$$E_O = 1 - e^{-\frac{1-O}{\sigma_O}} \tag{11}$$

4. E_C. The error C is defined as $C = \frac{\epsilon^2}{m}$, where ϵ is the error in the fit error and m is the total number of points:

$$E_C = 1 - e^{-\frac{C}{\sigma_C}} \tag{12}$$

Where $\sigma_A, \sigma_S, \sigma_O, \sigma_C$ are weighting factors for each criterion.

5 Experimental results

To determine whether radiation promotes aberrant ECM interactions we examined integrin and E-cadherin localization in preneoplastic human cells surviving radiation. Integrins are a family of epithelial receptors for the ECM, while E-cadherin maintains normal cell-cell interactions and architecture. We used the HMT-3522 (S1) human breast cell line cultured within a reconstituted ECM. These cells are genomicaly unstable but phenotypically normal in that

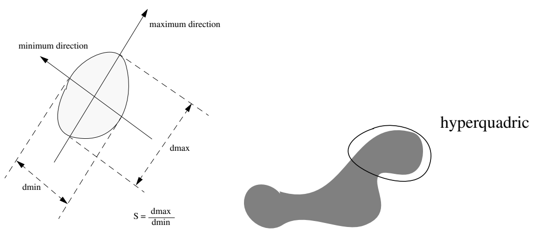

(a) (b)

Figure 9: Evaluation Criteria. (a) Shape rate; (b)Overlap rate.

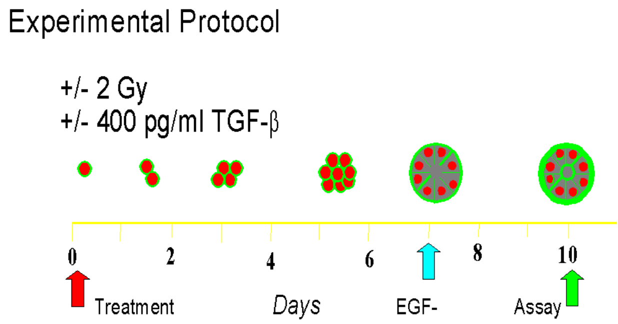

Figure 10: Experimental protocol for *invitro* treatment of a colony.

they recapitulate normal mammary architecture in the form of a multicellular, 3-dimensional acinus. These clusters express integrins in a polarized fashion and develop an organized ECM over the course of 7-10 days in culture.

We examined the consequences of exposing these cells to ionizing radiation and a protein modifier known as TGF- as shown in Figure 10. Antibodies to E-cadherin, 1 integrin or 6 integrin were detected using a green fluorescent label while nuclei were counterstained with a red fluorescent DNA dye. These were imaged using confocal fluorescence microscopy and were recorded using a 12-bit CCD camera. Cells that survived either 2 Gy or TGF- (400 pg/ml) exhibited decreased 1 or 6 integrin localization, respectively. However when cells were exposed to both radiation and TGF- , additional perturbations were noted. The clusters were disorganized, did not polarize the integrins at the cell surface and failed to express E-cadherin, indicative of a lack of structural organization. An example of the untreated cells is shown in Figure 11a, which is stained for 1 integrin (green) with red nuclei. Comparing this sample to Figure 11b, which is a colony of cells that were irradiated and treated with TGF- ; shows that the localization of 1 integrin is perturbed, as is the organization of the cells.

To test whether these observations represented a statistically significant event in the general population, the organization of the cells were quantified in the population using the nuclear segmentation algorithm outlined in this section. A database of images were used and the analysis confirmed the impact of radiation and TGF- on organization of a colony over the data set. A pair of images from untreated and treated samples, their segmentation, and organization is shown in Figure ??.

6 Conclusion

In the post-genome sequencing era, quantitative imaging of complex biological materials is a critical problem. Currently, sequential measurements ob-

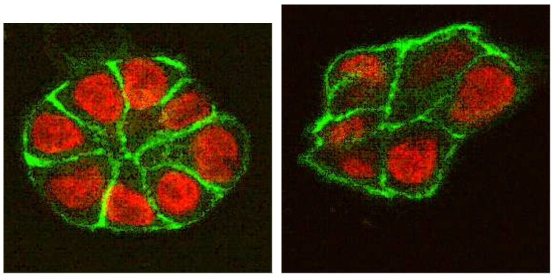

(a) (b)

Figure 11: Organization of a colony as a result of radiation and TGFβ treatment: (a) untreated sample maintains symmetry along the lumen; (b) treated sample looses its symmetric organization.

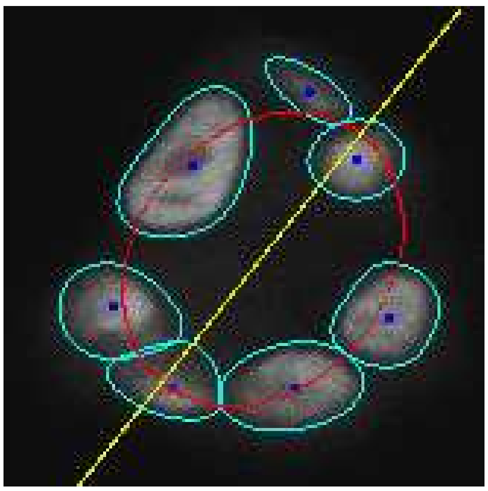

Figure 12: Normal growth and organization of a colony after 7-10 days.

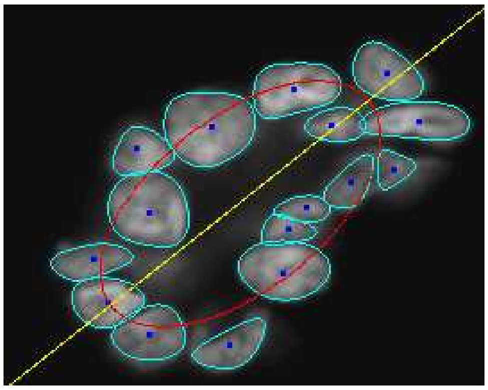

Figure 13: Organization of a colony after treatment indicates lack of symmetry around the lumen. Nuclei are segmented, represented with hyperquadrics, and a measure of symmetry by fitting an ellipse is measured.

tained with different microscopy techniques preclude detailed analysis of multidimensional responses (e.g. time and space). Quantification of spatial and temporal concurrent behavior of multiple markers in large populations of multicellular aggregates is hampered by labor intensive methods, a lack of quantitative tools and the inability to index information. Ideally one would track the kinetics and quantities of multiple target proteins, their cellular context and morphological features in 3-dimensions using large populations. There are several thousand antibodies and reagents for differentiating specific protein components of cells. Of these a large number are involved in signaling pathways, and many can discriminated between functional activation of a protein caused by modifications such as phosphorylation status, protein conformation and complex formation. However, these pathways are currently not well understood, due to the complexity of the potential events and lack of information regarding where and when a protein is actively participating in signaling. Inherent biological variability and genomic instability are additional factors that support the requirement for large population analysis. BioSig informatics approach to microscopy and image analysis can be used to build a more detailed picture of the signaling that occurs between cells, as a result of an exogenous stimulus such as radiation, or as a consequence of endogenous programs leading to biological functions.

References

[1] A. Amini, T. Weymouth, and R. Jain. Using dynamic programming for solving variational problems in vision. *IEEE Transactions on Pattern Analysis and Machine Intelligence*, pages 855–867, 1990.

[2] S. Han, D. Goldgof, and K. Bowyer. Using hyperquadric for shape recovery from rane data. In *Proceedings of the IEEE International Conference on Computer Vision*, pages 292–296, 1993.

[3] A. Hanson. Hyperquadrics: smoothly deformable shapes with convex polyhedral bounds. *Computer Vision, Graphics, and Image Processing*, 44:191–210, 1988.

[4] Y. Jin, Jayasooriah, and R. Sinniah. Clump splitting through concavity analysis. *Pattern Recognition*, 15:1013–1018, 1994.

[5] S. Kumar, S. Han, D. Goldgof, and K. Boeyer. On recovering hyperquadrics from range data. *IEEE Transactions on Pattern Analysis and Machine Intelligence*, 17(11):1079–1083, 1995.

[6] O. Monga, N. Ayache, and P. Sander. From voxel to intrinsic surface features. *Image and Vision Computing*, 10(6), 1992.

[7] O. Monga, S. Benayoun, and O. Faugeras. From partial derivatives of 3d density images to ridge lines. In *Proceedings of the Conference on Computer Vision and Pattern Recognition*, pages 354–359, 1992.

[8] B. Parvin, J. Taylor, and et al. Deepview: A channel for distributed microscopy. 1999.

[9] W. Press, S. Teukollsky, W. Vetterling, and B. Flannery. *Numerical Recipes in C*. Cambridge Unvi. Press, 1992.

[10] Bellman R. *Dynamic Programming*. Princeton University Press, 1957.

[11] M. Sonka, V. Hlavac, and R. Boyle. *Image Processing analysis and Machine Vision*. Chapman & Hall, 1995.

[12] H. Talbot and I Villalobos. Binary image segmentation using weighted skeletons. *SPIE Image algebra and morphological image processing*, 1769:393–403, 1992.

[13] J. Thirion. New feature points based on geometric invariants for 3d image registration. *International Journal of Computer Vision*, 18(2):121–137, 1996.

[14] J. Thirion and A. Gourdon. The 3d matching lines algorithm. *Graphical Models and Image Processing*, 58(6):503–509, 1996.

[15] W. Wang. Banary image segmentation of aggregates based on polygonal approximation and classification of concavities. *Pattern Recognition*, 31(10):1502–1524, 1998.